Hindawi
Mathematical Problems in Engineering
Volume 2018, Article ID 7480602, 16 pages
https://doi.org/10.1155/2018/7480602

Research Article

Online State of Charge Estimation for Lithium-Ion Battery by Combining Incremental Autoregressive and Moving Average Modeling with Adaptive H-Infinity Filter

Zheng Liu[1,2] **Xuanju Dang**[1] **and Hanxu Sun**[3]

[1]*School of Electronic and Automation, Guilin University of Electronic Technology, Guilin 541004, China*
[2]*School of Electronic and Automation, Guilin University of Aerospace Technology, Guilin 541004, China*
[3]*School of Automation, Beijing University of Posts and Telecommunications, Beijing 100876, China*

Correspondence should be addressed to Xuanju Dang; xjd69@163.com

Received 10 April 2018; Revised 3 June 2018; Accepted 24 June 2018; Published 9 July 2018

Academic Editor: Francesc Pozo

Copyright © 2018 Zheng Liu et al. This is an open access article distributed under the Creative Commons Attribution License, which permits unrestricted use, distribution, and reproduction in any medium, provided the original work is properly cited.

The state of charge (SOC) estimation is one of the most important features in battery management system (BMS) for electric vehicles (EVs). In this article, a novel equivalent-circuit model (ECM) with an extra noise sequence is proposed to reduce the adverse effect of model error. Model parameters identification method with variable forgetting factor recursive extended least squares (VFFRELS), which combines a constructed incremental autoregressive and moving average (IARMA) model with differential measurement variables, is presented to obtain the ECM parameters. The independent open circuit voltage (OCV) estimator with error compensation factors is designed to reduce the OCV error of OCV fitting model. Based on the IARMA battery model analysis and the parameters identification, an SOC estimator by adaptive H-infinity filter (AHIF) is formulated. The adaptive strategy of the AHIF improves the numerical stability and robust performance by synchronous adjusting noise covariance and restricted factor. The results of experiment and simulation have verified that the proposed approach has superior advantage of parameters identification and SOC estimation to other estimation methods.

1. Introduction

In the field of electric vehicles (EVs), the Lithium-ion batteries have been widely researched and quickly developed in battery management system (BMS) at present [1, 2]. Onboard BMS is used to guarantee the safety of the work and reliable battery application in high energy EVs. An accurate SOC is one of the core functions in the BMS, which provides the fundamental principle of the battery available capacity for maintaining a longer lasting time. In many cases, other additional functions in the BMS also rely on precise SOC estimation [3, 4]. Beyond that, the accurate SOC estimation is dramatically impacted on the time scale for charge and discharge; otherwise overcharge and overdischarge will have serious and negative impact on battery life time and EVs driving safety. Therefore, a reliable and high-precision SOC prediction method is significant for the optimization of BMS in EVs control strategy [5, 6].

Various efforts focusing on the estimation of SOC have been made in the last few years. In general, the known estimation methods could be classified into two categories: model-free methods and model-based methods. The classical model-free approach is the Ampere-Hour integral (AH) [7, 8] that is the remainder charge is equal to the integral of charge or discharge current. Nevertheless, two preconditions should be satisfied simultaneously, which are exact initialization SOC data and the high-precision sensor. In the process of current integration, AH suffers from the accumulative error and rounding error in disturbances condition, such as current or temperature fluctuations, etc. The OCV measurement [9–11] also is commonly used technique for SOC estimation based on the nonlinear OCV-SOC fitting curve under incremental OCV test or low-current OCV test. However, it is a poor choice for real-time SOC estimation in EVs ongoing application because the battery's steady state is not achieved until the long rest time. In addition, the machine learning

approach (MLA), such as the artificial neural network (ANN) [12, 13], the fuzzy logic [14, 15], and the support vector machine (SVM) [16, 17], takes a Lithium-ion battery as a black-box model. Although MLA does not require the exact current-voltage information of battery dynamics, it is almost impossible to cover all the battery loading data through studying the training dataset. And because of large amount of time consumption, it is not a better design for BMS.

In the model-based estimation methods, the choice of model should be firstly determined. Equivalent-circuit model (ECM) is the most widely used model for battery applications. The ECM can be classed as one reduced form of complex electrochemical model, which is applied to approximate the battery dynamic behavior with identified parameters. In [18], the dynamic response of battery can be simulated by one-order ECM, and a recursive least squares (RLS) method is used for parameters identification. Other types of ECM which introduce two or three order RC network are presented in [19, 20]. Although multiorder ECM can lead to better performance in representing battery dynamic behavior than the one-order ECM, the more ECM parameters need to be identified with deepening of algorithm complexity. In [21, 22], an additional noise is added to one-order ECM, but the RLS with constant forgetting factor may encounter the difficulties of compromise between stability and convergence. Therefore, the effective ECM is largely dependent on the balance between complexity and precision of corresponding algorithm.

In the ECM-based state observers, the flexible usage of Kalman filter has been generally accepted for its better performance of optimal estimation, which assumes some special properties of the problem formulation, such as model error-free and known noise statistics. For example, the extended Kalman filter (EKF) algorithm is applied for Lithium-ion battery state estimation to obtain a desired resistance estimation result [23, 24]. But with the strong fluctuating current problems and the undeniable error of the first-order Taylor series approximation, the convergence speed of EKF is slow or even cannot get a convergence solution in time. The unscented Kalman filter (UKF) with unscented transformation (UT) method is utilized to handle the SOC estimation problem in strong nonlinear battery systems [25, 26], and the estimation results show that the UKF has better robustness and higher precision than the EKF. The adaptive EKF (AEKF) and adaptive UKF (AUKF) based on the dynamic adaptive strategy of adjusting noise were adopted in state estimator to achieve the goal of high-precision and better stability than EKF and UKF [27, 28]. In [29–33], an H-Infinity Filter (HIF) based on the mini-max residual error criterion observer is designed for model parameters identification and state estimation, which has more robust to model error uncertainty without assumptions of accurate battery model. Generally, the HIFs are more robust than KFs [34, 35], but they do not sufficiently consider the effect of the error of process noise and measurement noise. In other words, the uncertain covariance of noise can result in unavoidable estimation error of the HIF. One common feather of the aforementioned methods is that

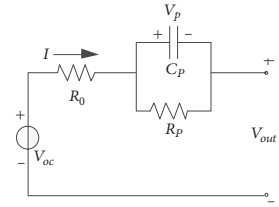

Figure 1: Schematic diagram of one-order ECM.

OCV can be calculated from OCV-SOC fitting model [23–35]. However, due to fitting error in OCV-SOC curve [9], any small perturbation in OCV calculation by OCV-SOC fitting model may cause a large deviation in SOC estimation, especially a wide flat area existing in the OCV-SOC curve with a strong nonlinear relationship.

The main contributions of this paper include the following: (1) a novel IARMA battery model based on VFFRELS method is designed to identify the battery model parameters; (2) an error compensation based independent OCV estimator is adopted to accurately capture the OCV; (3) with design and application of adaptive HIF (AHIF) including noise covariance and restricted factor adjustment to the proposed model, the SOC is directly estimated with reasonable performance. Compared with the wide usage of AEKF, the proposed method has the features of accurate model, strong robustness, and high precision.

The remainder of this paper is arranged as follows. Section 2 presents details of the IARMA-based battery ECM and the model parameters identification based on VFFRELS algorithm. The error feed forward compensation based independent OCV estimator is analyzed in Section 3. Then based on the IARMA battery model and identified parameters, an AHIF-based SOC estimator is proposed in Section 4. Section 5 shows the experimental and simulation results under the different conditions. Finally, some conclusions are drawn in Section 6.

2. Battery Model and Parameters Identification

2.1. Battery Model Derivation. In a simplified model sense, the dynamic electrical characteristic of the Lithium-ion battery can be commonly represented by the one-order ECM [18], as shown in Figure 1.

One-order ECM is expressed as follows:

$$\frac{dV_p(t)}{dt} = -\frac{V_p(t)}{R_pC_p} + \frac{I(t)}{C_p}$$
$$V_{out}(t) = V_{oc}(t) - R_0 I(t) - V_p(t) \quad (1)$$

where $V_{oc}(t)$ is used to describe the SOC dependent OCV which is associated with OCV-SOC fitting curve, R_0 indicates the ohmic resistance, the parallel R_pC_p composed of a polarization resistance and a polarization capacitance, $V_p(t)$ represents polarization voltage across parallel R_pC_p, $I(t)$ is the current in the charging and discharging status, and $V_{out}(t)$ represents the terminal voltage.

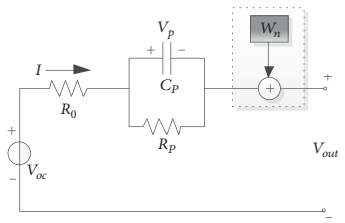

Figure 2: Schematic diagram of improved one-order ECM.

The one-order ECM cannot completely describe battery dynamic nature, since the model random noise characteristic is not included in (1). As illustrated in Figure 2, a colored noise w_n has been added as a compensation module in one-order ECM, and w_n is to cover the random error which is not considered in the one-order ECM [21, 22].

Based on Figure 2, the mathematical model of one-order ECM with additive colored noise can be derived as

$$\frac{dV_p(t)}{dt} = -\frac{V_p(t)}{R_pC_p} + \frac{I(t)}{C_p}$$
$$V_{out}(t) = V_{oc}(t) - R_0 I(t) - V_p(t) + w_n(t) \tag{2}$$

In (2), the colored noise $w_n(t)$ is a noise sequence driven by a series of white noise sequence, and $e(t), e(t-1), \cdots, e(t-n_c)$ are its regression of data; thus,

$$w_n(t) = e(t) + c_1 e(t-1) + \cdots + c_n e(t-n_c) \tag{3}$$

The nonlinear time series model is adopted to analyze battery ECM; let u and y be the charge/discharge current and the terminal voltage of battery ECM, respectively. The ECM in (2) to be identified can be redefined as a multivariable regression expression:

$$y(k) = a_1 y(k-1) + a_2 y(k-2) + \cdots + a_p y(k-p+1) + b_1 u(k-1) + b_2 u(k-2) + \cdots + b_q u(k-q+1) + w_n(k) \tag{4}$$

where p and q are the orders of regression expression; $a_1, a_2, \ldots a_p$ and $b_1, b_2, \ldots b_q$ are the undetermined coefficient.

2.2. Parameters Identification. By comparing (2) with (4), the polarization voltage is firstly needed to eliminate from (2). The discretization form of (2) by bilinear transformation method: $s = (2/T_s)((1-z^{-1})/(1+z^{-1}))$ (z is the discretization operator) is given as follows:

$$V_{out}(k) = a_1 V_{out}(k-1) + b_1 I(k) + b_2 I(k-1) + \left[V_{oc}(k) - a_1 V_{oc}(k-1)\right] + w_n(k)$$
$$w_n(k) = e(k) + c_1 e(k-1) + \cdots + c_n e(k-n) \tag{5}$$

where $V_{oc}(k)$, $V_{out}(k)$ and $I(k)$ is the OCV, terminal voltage, and load current at the kth sampling time, respectively, and the coefficient can be obtained by $a_1 = (2R_pC_p - 1)/(1 + 2R_pC_p)$, $b_1 = -(2R_0R_pC_p + R_0 + R_p)/(1 + 2R_pC_p)$, $b_2 = (2R_0R_pC_p - R_0 - R_p)/(1 + 2R_pC_p)$. Then R_0, R_p, and C_p can be obtained according to the inverse equations of a_1, b_1, and b_2; thus, $R_0 = (b_2 - b_1)/(1 + a_1)$, $R_p = 2(b_2 + a_1b_1)/(a_1^2 - 1)$, $C_p = -(a_1 + 1)^2/[4(b_2 + a_1b_1)]$.

By comparing (5) with (4), the immeasurable part $[V_{oc}(k) - a_1 V_{oc}(k-1)]$ is assumed as the residual model error (RME) of autoregression (AR) model. Since the above colored noise sequence $w_n(k)$ can be used as a MA process, (5) can be considered as an autoregressive moving average model (ARMA) with external input system.

Similarly, the terminal voltage of the previous step $(k-1)$ could be expressed as follows:

$$V_{out}(k-1) = a_1 V_{out}(k-2) + b_1 I(k-1) + b_2 I(k-2) + \left[V_{oc}(k-1) - a_1 V_{oc}(k-2)\right] + w_n(k-1)$$
$$w_n(k-1) = e(k-1) + c_1 e(k-2) + \cdots + c_n e(k-n-1) \tag{6}$$

By subtracting (6) from (5), the incremental-based ARMA (IARMA) equation will be derived as follows:

$$\Delta V_{out}(k) = a_1 \Delta V_{out}(k-1) + b_1 \Delta I(k) + b_2 \Delta I(k-1) + \Delta\left[V_{oc}(k) - a_1 V_{oc}(k-1)\right] + \Delta w_n(k)$$
$$\Delta w_n(k) = \Delta e(k) + c_1 \Delta e(k-1) + \cdots + c_n \Delta e(k-n) \tag{7}$$

where $\Delta V_{out}(k)$, $\Delta I(k)$, $\Delta[V_{oc}(k) - a_1 V_{oc}(k-1)]$ and $\Delta e(k)$ are calculated as $V_{out}(k) - V_{out}(k-1)$, $I(k) - I(k-1)$, $[V_{oc}(k) - a_1 V_{oc}(k-1)] - [V_{oc}(k-1) - a_1 V_{oc}(k-2)]$ and $\Delta e(k) = e(k) - e(k-1)$, respectively. Meanwhile the immeasurable part $\Delta[V_{oc}(k) - a_1 V_{oc}(k-1)]$ is also assumed as the RME of IARMA model [36, 37].

If the parameters identification algorithm is based on (5) or (7), whether the RME can be ignored compared with terminal voltage in (5) or (7) is the first consideration. The detailed property of two RME of ARMA and IARMA will be analyzed as a quantifiable form in Section 5.

From (7), it is seen that y and u of the IARMA model are ΔV_{out} and ΔI, respectively. In accordance with nonlinear regression mode principle, (7) can be rewritten as least-squares form:

$$\Delta V_{out}(k) = \varphi^T(k)\,\theta(k) + \nu(k) \tag{8}$$

where

$$\varphi(k) = \left[\Delta V_{out}(k-1)\ \ \Delta I(k)\ \ \Delta I(k-1)\ \ 1\ \ \Delta e(k-1) \cdots \Delta e(k-n)\right]$$
$$\theta(k) = \left[a_1\ \ b_1\ \ b_2\ \ \Delta\left[V_{oc}(k) - a_1 V_{oc}(k-1)\right]\ \ c_1 \cdots c_n\right]^T$$
$$\Delta e(k) = \left[e(k) - e(k-1)\right]$$
$$\nu(k) = \Delta e(k) \tag{9}$$

In (8), $\theta(k)$ is the unknown parameters set, and $\varphi(k)$ is the coefficient determined by known variable. Since the

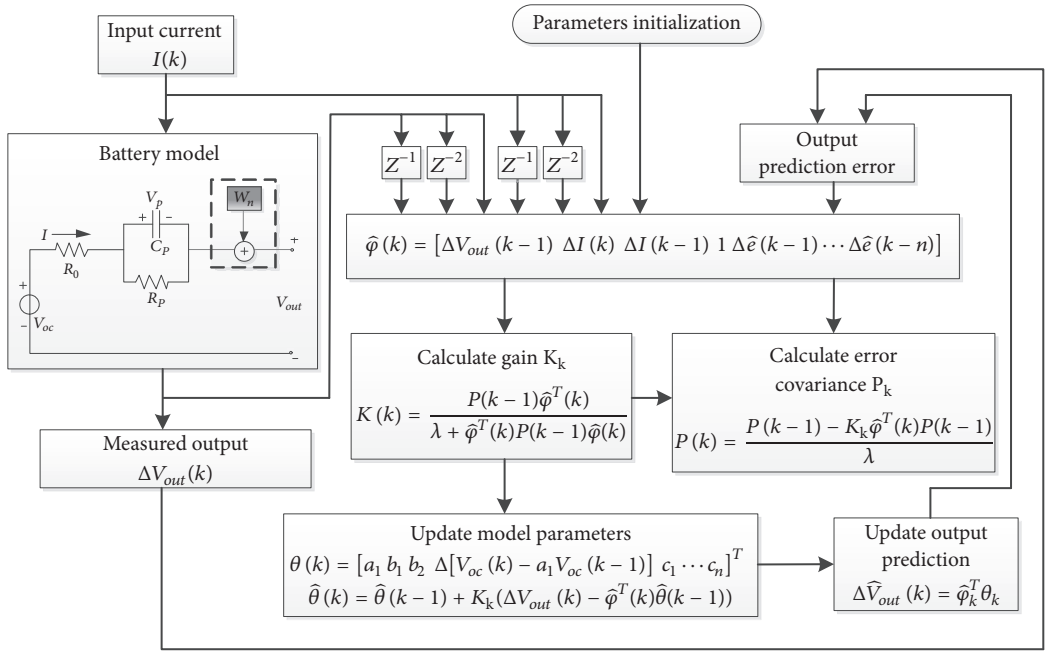

Figure 3: Parameters identification algorithm for the improved one-order ECM.

time sequence of $\Delta e(k)$ is immeasurable, $\varphi(k)$ cannot be got directly; therefore some traditional least squares (LS) series online identification algorithms are unable to identify $\theta(k)$. Accordingly, the RELS algorithm [21, 22] is introduced to identify the immeasurable noise terms first. Based on (5) and (8), $e(k)$ can be approximated to the difference between measured terminal voltage and identified terminal voltage; meanwhile, $\Delta e(k)$ can be approximated to the difference between measured differential terminal voltage and identified differential terminal voltage, as follows.

$$\begin{aligned}\hat{e}(k-i) &= V_{out}(k-i) - \hat{V}_{out}(k-i)\\ \Delta\hat{e}(k-i) &= \Delta V_{out}(k-i) - \Delta\hat{V}_{out}(k-i)\\ &= \Delta V_{out}(k-i) - \hat{\varphi}(k-i)^T\hat{\theta}(k-i)\end{aligned} \tag{10}$$

where $i = 1, 2, ..., n$

Thereafter, $\Delta e(k)$ can be replaced with $\Delta\hat{e}(k)$, and we define the following:

$$\begin{aligned}&\hat{\varphi}(k)\\ &= [\Delta V_{out}(k-1)\ \ \Delta I(k)\ \ \Delta I(k-1)\ \ 1\ \ \Delta\hat{e}(k-1)\cdots\Delta\hat{e}(k-n)]\end{aligned} \tag{11}$$

where $\hat{e}(1) = \hat{e}(2) = ... = \hat{e}(n) = e(0)$, $e(0)$ is a given initial value of the noise sequence.

With the updated $\hat{\varphi}(k)$ by (11), the regression data of colored noise $w_n(k)$ can be obtained by (5)-(10). The procedures of IARMA and RELS based identification method are illustrated in Figure 3.

The RELS is used to solve the regression model described in Figure 3. However, the RELS with constant forgetting factor λ may encounter the difficulties of balancing between stability and convergence if the model parameters change with different rates. The battery dynamics nature of one-order ECM can be distinguished into two slow parameters and one fast parameter [38–40]. The fast parameter represents internal ohmic resistance R_0, while the slow parameters include R_p and C_p. In this regard, a large forgetting factor should be assigned to the parameters changing slowly to guarantee the stability of the algorithm, while a small forgetting factor is more appropriate for the tracking of fast varying parameter. In seeking to address this problem, the VFFRELS with multiple forgetting factors [41–43] for identification is applied in this paper. With the VFFRELS, the forgetting factors can be decoupled and tuned separately to improve the parameters stability and tracking accuracy of SOC estimation.

3. Independent OCV Estimator with Error Compensation

3.1. OCV Estimator. In this section, an independent OCV estimator is introduced. The OCV is observed with the aid of battery ECM characterization. $V_p(t)$ in (1) can be rewritten in the discrete-time form as follows:

$$\begin{aligned}V_p(k) &= e^{-1/R_pC_p}V_p(k-1)\\ &\quad + \left(1 - e^{-1/R_pC_p}\right)R_pI(k-1)\end{aligned} \tag{12}$$

From (1), obviously $V_p(k)$ can be expressed in the following discrete-time relationship as follows:

$$V_p(k-1) = V_{oc}(k-1) - V_{out}(k-1) - R_0 I(k-1) \quad (13)$$

Substituting (13) into (12) yields the following:

$$\begin{aligned} V_{oc}(k) &= e^{-1/R_pC_p} V_{oc}(k-1) \\ &\quad - e^{-1/R_pC_p}\left(V_{out}(k-1) + R_0 I(k-1)\right) \\ &\quad + \left(1 - e^{-1/R_pC_p}\right) R_p I(k-1) + V_{out}(k) \\ &\quad + R_0 I(k) \end{aligned} \quad (14)$$

Since the OCV can be described as a slow time-varying variable, then the OCV estimation can be solved by the expression of R_0, R_p, and C_p, as follows:

$$\widehat{V}_{oc}(k) = \frac{V_{out}(k) + R_0 I(k) - e^{-1/R_pC_p}\left(V_{out}(k-1) + R_0 I(k-1)\right) + \left(1 - e^{-1/R_pC_p}\right) R_p I(k-1)}{1 - e^{-1/R_pC_p}} \quad (15)$$

3.2. OCV Error Compensation. The OCV-SOC curve can be easily obtained under incremental OCV test and low-current OCV test [35]. The nonlinear characteristic relationship of OCV-SOC fitting model is built in processing the experimental data by the polynomial curve fitting methods.

$$V_{oc}(k) = \sum_{i=0}^{N} b_i SOC(k)^i \quad (16)$$

where b_i is the polynomial fitting coefficient, N is the order of fitting model, and N is set to 8.

The direct calculation of OCV by OCV-SOC fitting model contains perturbations due to the existence of fitting error. Therefore, the OCV error will largely decline the accuracy of SOC estimation. Besides, there exists a flat area in the OCV-SOC curve with a strong nonlinear relationship when the value of SOC varies from 0.2 to 0.8 [18]. Even if the measurement error of voltage or current is relatively slight, the OCV error can lead to a relatively large OCV-based SOC estimation error. To solve this problem, OCV is corrected with two compensations by considering the intrinsic OCV variation.

First, the residual error of terminal voltage is introduced to approximately describe the behaviors of deviation of OCV. A microadjustment factor is adopted for compensating error caused by nonequivalence behavior between terminal voltage and OCV. The simple correction formula is shown as follows:

$$\Delta\widehat{V}_{oc1}(k) = \alpha_1\beta_1\left(V_{out}(t) - \widehat{V}_{out}(t)\right) \quad (17)$$

where $\Delta\widehat{V}_{oc1}$ is used as first compensation, microadjustment factor α_1 is below a certain range ($0 < \alpha_1 < 1$ in this paper), and the proportion coefficient β_1 is 10^2. The microadjustment factor α_1 is determined by the slope of OCV-SOC curve.

Next, due to the fitting error in OCV-SOC fitting model, the second appropriate compensation is necessary to further eliminate OCV error. The second compensation $\Delta\widehat{V}_{oc2}$ is adopted to reduce the fitting error in OCV-SOC fitting model. $\Delta\widehat{V}_{oc2}$ for OCV is equal to the behaviors of the deviation between $\widehat{V}_{oc}(k)$ by OCV estimator and $V_{oc}(k)$ by OCV-SOC fitting model.

The block diagram of two OCV compensation methods is shown in Figure 4. The terminal voltage estimation value ($\widehat{V}_{out}$) and OCV estimation value ($\widehat{V}_{oc1}$) are utilized to the get corresponding compensation factor ($\Delta\widehat{V}_{oc1}$ and $\Delta\widehat{V}_{oc2}$) which are employed to correct the OCV by the feed forward method.

4. Adaptive HIF Based SOC Estimator

4.1. HIF with Tunable Restricted Factor. In the strict sense, the accurate ECM and noise statistics quantity is the precondition to bring into playing KFs advantages. However, the KFs cannot be guaranteed to work stably all the time when these conditions cannot be satisfied. The H-Infinity Filter (HIF) based on the game theory which is designed to minimize the maximum estimation error can make up for the lack of the precondition; thus it is common in resolving the problem of system identification in [29–31]. The SOC estimation in [32–35] shows that the HIF can provide the impressive results with inexact or unknown initialized state. The cost function of HIF is defined as follows:

$$\begin{aligned} J_1 &= \frac{\sum_{k=0}^{N-1} \|x_k - \widehat{x}_k\|_{S_k}^2}{\|x_0 - \widehat{x}_0\|_{P_0^{-1}}^2 + \sum_{k=0}^{N-1}\left(\|w_k\|_{Q_k^{-1}}^2 + \|v_k\|_{R_k^{-1}}^2\right)} \\ &= \frac{\sum_{k=0}^{N-1}(x_k - \widehat{x}_k) S_k (x_k - \widehat{x}_k)^T}{(x_0 - \widehat{x}_0) P_0^{-1} (x_0 - \widehat{x}_0)^T + \sum_{k=0}^{N-1}\left(w_k Q_k^{-1} w_k^T + v_k R_k^{-1} v_k^T\right)} \end{aligned} \quad (18)$$

where x_k is the state value and $\widehat{x}_k$ is state estimation; x_0 and $\widehat{x}_0$ are the initial states value. w_k and v_k are the process noise vector and measurement noise vector, respectively. P_0, Q_k, R_k, and S_k are the symmetric positive definite matrixes.

Further, since it is difficult to directly minimize cost function J_1, a user-specified restricted factor γ^2 which has important influence on the precision and robustness is presetting to guarantee an optimized boundary constrained condition, making sure that J_1 satisfies $J_1 < \gamma^2$. In [32, 33], the restricted factor γ^2 is set to a fixed value based on the engineering practice experience, and three restricted factors of 1.531, 1.048, and 1.003 are adopted in state estimation. For ensuring both robustness and precision, the self-adapting restricted factor is incorporated into HIF by innovation mechanism.

By applying the matrix inversion lemma to $P_{k|k}$, we obtain

$$P_{k|k}^{-1} = L_k^T L_k \left(P_{k|k-1}^{-1} + A_k^T A_k\right)^{-1} - \gamma^{-2} I \quad (19)$$

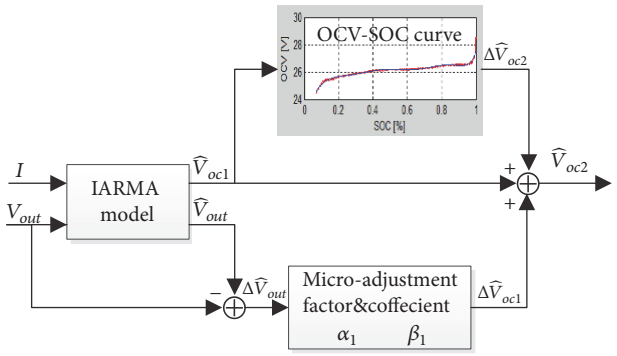

Figure 4: The block diagram of OCV error compensation algorithm.

As $P_{k|k}$ is a covariance matrix, it therefore should be positive definiteness. This means that

$$L_k^T L_k \left(P_{k|k-1}^{-1} + A_k^T A_k\right)^{-1} - \gamma^{-2} I \geq 0 \tag{20}$$

In other words, the restricted factor γ should satisfy

$$\gamma^2 \geq \lambda_{\max}\left(L_k^T L_k \left(P_{k|k-1}^{-1} + A_k^T A_k\right)^{-1}\right) \tag{21}$$

where $\lambda_{\max}(A)^{-1}$ denotes the greatest eigenvalue of matrix $(A)^{-1}$; therefore, self-adapting method for restricted factor γ is

$$\gamma = \alpha_2 \sqrt{\lambda_{\max}\left(L_k^T L_k \left(P_{k|k-1}^{-1} + A_k^T A_k\right)^{-1}\right)} \tag{22}$$

where α_2 is used to correct γ and $\alpha_2 > 1$; the quadratic sum of innovation error e_k from (27) is used as estimation error $e_k^T e_k$. As the restricted factor γ is inversely proportional to the estimation error, the correction coefficient expression is shown as follows:

$$\alpha_2 = 1 + \frac{\beta_2}{\sqrt{e_k^T e_k}} \tag{23}$$

where β_2 is an unknown coefficient associated with experiments and $\beta_2 > 0$, once β_2 is determined, the correction coefficient α_2 is only dependent on innovation error e_k. That is, the relationship between restricted factor γ and estimation error $e_k^T e_k$ can be quantitatively depicted by (22)-(23).

The calculation process of the discrete-time HIF with tunable restricted factor is shown as follows:

Step 1: Initialization

$$\begin{aligned}&\text{State: } X_0 = (SOC_0 \;\; U_{p,0})\\ &\text{Restricted factor: } \gamma_0\\ &\text{Symmetric positive definite matrixes: } P_0, S_0, Q_0, R_0\end{aligned} \tag{24}$$

Step 2: State estimation

$$\begin{aligned}&\text{Prior state estimation: } \widehat{X}_{k|k-1} = A_{k|k-1}\widehat{X}_{k-1|k-1} + B_{k-1}I_{k-1}\\ &\text{Prior state covariance: } P_{k|k-1} = A_{k|k-1}P_{k-1|k-1}A_{k|k-1}^T + Q_{k-1}\\ &\text{Symmetric positive definite matrix update: } \overline{S}_k = L_k^T S_k L_k\end{aligned} \tag{25}$$

Step 3: Measurement correction

$$\begin{aligned}&\text{Gain matrix update: } K_k = P_{k|k-1}\left(I - \gamma S_k P_{k|k-1} + C_k^T R_k^{-1} C_k P_{k|k-1}\right)^{-1} C_k^T R_k^{-1}\\ &\text{Posterior state update: } \widehat{X}_{k|k} = \widehat{X}_{k|k-1} + K_k\left(y_k - C_k\widehat{X}_{k|k-1} - D_k I_k\right)\\ &\text{Posterior state covariance update: } P_{k|k} = P_{k|k-1}\left(I - \gamma\overline{S}_k P_{k|k-1} + C_k^T R_K^{-1} C_k P_{k|k-1}\right)^{-1} + R_k\end{aligned} \tag{26}$$

Tunable restricted factor update:

$$\begin{aligned}\gamma_k &= \alpha_2\sqrt{\lambda_{\max}\left(L_k^T L_k\left(P_{k|k}^{-1} + A_k^T A_k\right)^{-1}\right)}\\ \alpha_2 &= 1 + \frac{\beta_2}{\sqrt{e_k^T e_k}}\end{aligned}$$

4.2. HIF with Adaptive Strategy. Multiple adaptive ways have integrated into original KFs such as the Bayes method, maximum likelihood criterion, correlation method, and covariance matching method. As mentioned before, the HIF approaches to KF when $\gamma \longrightarrow \infty$. Hence it can be concluded that the noise covariance matrix Q_k and R_k in HIF play the similar role in the KFs which should be adjusted properly. Therefore, an adaptive HIF with the maximum likelihood criterion [34] is designed to update the noise covariance at each stage of measurement correction to strengthen its jamming immunity of SOC estimation.

According to (2), the innovation error can be written as an expression of difference between measurement estimation and true measurement value:

$$e_k = y_k - \left(C_k \hat{x}_{k|k-1} + D_k I_k\right) = C_k \left(x_k - \hat{x}_{k|k-1}\right) + v_k \quad (27)$$

The measurement innovation covariance is deduced through the use of probability theory.

$$\begin{aligned} P_{e_k} &= E\left[\left(C_k \left(x_k - \hat{x}_{k|k-1}\right) + v_k\right)\right. \\ &\quad \left. \cdot \left(C_k \left(x_k - \hat{x}_{k|k-1}\right) + v_k\right)^T\right] = C_k P_{k|k-1} C_k^T + \hat{R}_k \end{aligned} \quad (28)$$

where P_{e_k} denotes the covariance of e_k, then the definition of innovation estimation variance $\hat{P}_{e_k}$ is introduced to describe P_{e_k} through using moving window method of innovation.

$$\hat{P}_{e_k} = \frac{1}{L} \sum_{j=k-L+1}^{k} \mathrm{e}_j \mathrm{e}_j^T \quad (29)$$

By combining (28) and (29), the following observation noise covariance equation can be drawn:

$$\hat{R}_k = \hat{P}_{e_k} - C_k P_{k|k-1} C_k^T \quad (30)$$

Similarly, the state noise w_k can be expressed as follows:

$$w_{k-1} = x_k - A_{k-1} x_{k-1} \quad (31)$$

Substituting the prior state estimation $\hat{x}_{k|k-1}$ into (31) yields

$$\begin{aligned} w_{k-1} &= x_k - A_{k-1} x_{k-1} \\ &= x_k - \hat{x}_{k|k-1} - A_{k-1}\left(x_{k-1} - \hat{x}_{k-1|k-1}\right) \\ &= x_k - \hat{x}_{k|k} - A_{k-1}\left(x_{k-1} - \hat{x}_{k-1|k-1}\right) \\ &\quad + \left(\hat{x}_{k|k} - \hat{x}_{k|k-1}\right) \\ &= \left(x_k - \hat{x}_{k|k}\right) - A_{k-1}\left(x_{k-1} - \hat{x}_{k-1|k-1}\right) + K_k e_k \end{aligned} \quad (32)$$

Based on the principle of orthogonality between the innovation and the residual, the state noise covariance $\widehat{Q}_k$ is taken on both sides of (32).

$$\begin{aligned} \widehat{Q}_k &= \mathrm{E}\left[w_k w_k^T\right] = \mathrm{E}\left[\left(\left(x_k - \hat{x}_{k|k}\right)\right.\right. \\ &\quad - A_{k-1}\left(x_{k-1} - \hat{x}_{k-1|k-1}\right) + K_k e_k\left)\left(\left(x_k - \hat{x}_{k|k}\right)\right.\right. \\ &\quad \left.\left. - A_{k-1}\left(x_{k-1} - \hat{x}_{k-1|k-1}\right) + K_k e_k\right)^T\right] = P_k \\ &\quad - A_{k-1} P_{k|k-1} A_{k-1}^T + K_k \hat{P}_{e_k} K_k^T \end{aligned} \quad (33)$$

Based on the adaptive strategy analysis, the adaptive iteration approach which is detailed in (30) and (33) is utilized to compensate for process and measurement noises uncertainties in HIF algorithm.

4.3. SOC Estimator Based on the AHIF. First, the ECM parameters and OCV are identified as two independent parameters set by using VFFRELS and compensation method in improved one-order ECM. Next, the HIF accompanied with tunable restricted factor and adaptive strategy is applied to SOC estimation. The formulas of state and observation are as follows:

$$\begin{aligned} X_k &= A_{k-1} X_{k-1} + B_{k-1} I_{k-1} + w_{k-1} \\ Y_k &= C_k X_k + D_k I_k + v_k \\ Z_k &= L_k X_k \end{aligned} \quad (34)$$

where $X = [SOC, U_p]$, Y_k is the terminal voltage, Z_k represents a linear combination of the state, and the user-defined matrix $L_k = [1, 0]$. The system matrixes A_k, B_k, C_k, D_k which describe the dynamics of the ECM are given as follows:

$$\begin{aligned} A_k &= \begin{bmatrix} 1 & 0 \\ 0 & e^{-\Delta t / R_p C_p} \end{bmatrix}, \\ B_k &= \begin{bmatrix} -\dfrac{\eta_i \Delta t}{C_n} \\ \left(1 - e^{-\Delta t / R_p C_p}\right) R_p \end{bmatrix}, \\ C_k &= \left[\left. \frac{dV_{oc}(SOC)}{dSOC} \right|_{SOC=SOC_{k|k-1}} \quad -1 \right], \\ D_k &= \left[-R_0\right] \end{aligned} \quad (35)$$

With the equations of state and observation above, the battery SOC is estimated by using the improved AHIF. The process of the HIF with tunable restricted factor for the SOC estimation can be seen in (24)-(26), the noise covariance adaptive adjusted strategy is given in (30) and (33), and the general flowchart of the IARMA-AHIF based parameters and SOC joint estimation method is illustrated in Figure 5. The SOC estimation is obtained by recursion procedure based on identified ECM parameters and OCV.

5. Results and Discussion

To evaluate the performance of parameters identification and SOC estimation, the 20Ah/24V Lithium-ion phosphate battery is selected as the test objects, in which the cathode and anode are formed from Lithium iron phosphate and graphite, respectively. In order to acquire high-precision experimental data such as charge/discharge current, voltage, available capacity, etc., the battery experimental platform is set up for the validation experiments. The reliable test platform is composed of a host computer which is used for data collection and data processing, a high precise power battery test system (Arbin Corp, EVTS) with the maximum charging/discharging current of 300A and maximum voltage

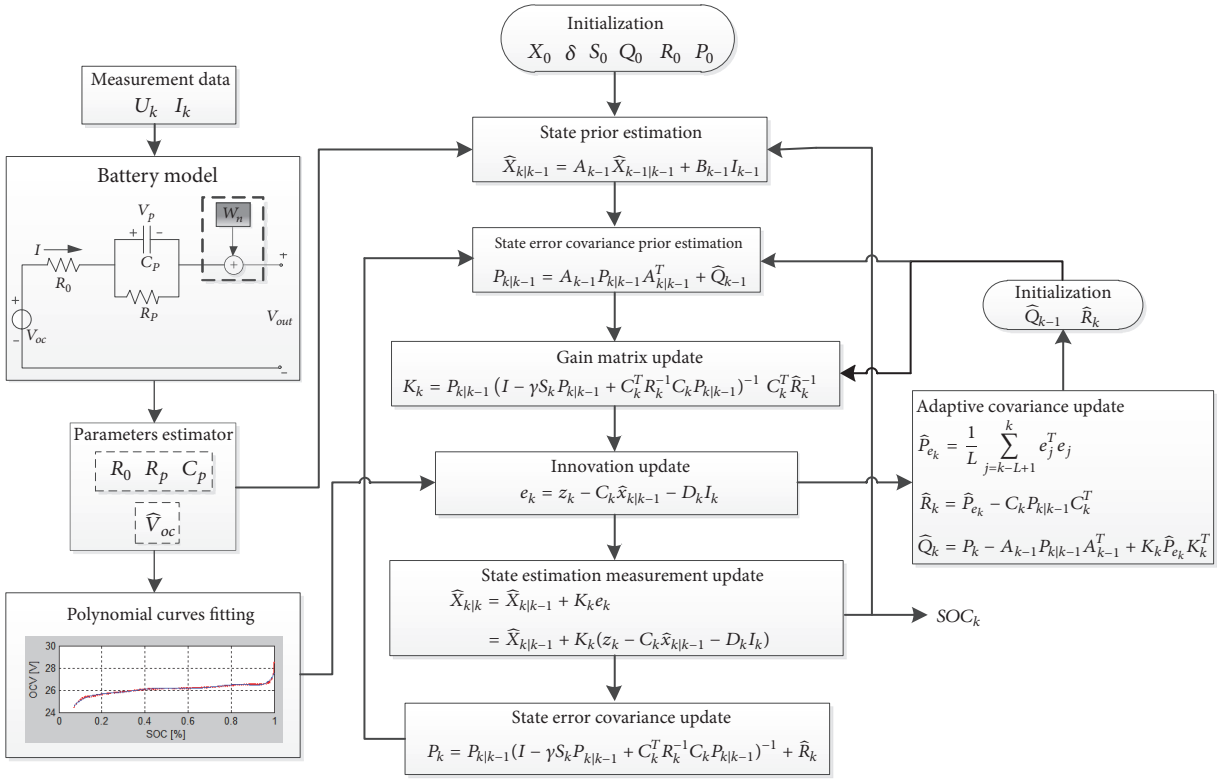

Figure 5: The flowchart of the IARMA-AHIF based SOC estimator.

of 400V, and a programmable temperature chamber to provide controllable temperature.

The data of two operating conditions including Dynamic Stress Test (DST) and Federal Urban Driving Schedule (FUDS) at a constant temperature 25°C for the battery are collected to evaluate the performance of model parameters identification and SOC estimation. In addition, the statistical index such as maximum absolute error (MAE) and average absolute error (AAE) are used to qualify performance of the identification and estimation algorithms.

5.1. Model Parameters Identification Results and Comparative Analysis. First, the Lithium-ion battery is fully charged by standard charging method, and then it is left to rest for one hour before being discharged in working condition. The discharge current-time distribution of the DST and FUDS cycle in which the duration of uninterrupted working condition is 35000 seconds is shown in Figure 6. With the data flows of collected discharge current and terminal voltage, the VFFRELS algorithm and IARMA model are combined to identify the ECM parameters and terminal voltage. The identification results of R_0, R_p, and C_p are shown in Figure 7.

As shown in Figures 7(a) and 7(b), the identification values of ECM parameters is able to converge to stable values rapidly in the DST and FUDS cycle, respectively. Among them, the ohmic resistance R_0 and the polarization resistance R_p exhibit the similar tendencies except for a little fluctuation. Specifically, R_0 keeps a higher stability and for the ohmic resistance is equal to the ratio of terminal voltage variation to transient current when the variable current is turned off. By contrast to R_0 and R_p, the polarization capacitance C_p varies significantly because R_p and C_p are direct correlation to intricate electrochemical activity. Although the introduction of multiorder ECM can lead to better stable R_p and C_p in representing battery dynamic characteristics than the one-order ECM in theory, the more ECM parameters need to be identified with increasing of algorithm complexity which is not suitable for real-time application. To summarize, R_0 and one-order R_pC_p of ECM have to real-time change with limited amplitude during operating condition to keep closer track of electrochemical activity.

With the identified R_0, R_p, and C_p, the terminal voltage as ECM observation is recursive obtained in each sampling period. Figures 8(a) and 8(b) demonstrate the two model-based measured and identified battery terminal voltages under DST cycle. The red line in Figure 8(a) is the ARMA-based estimation value and the blue line denotes the IARMA-based estimation value. As indicated in Figure 8(b), the AAE of ARMA and IARMA are 0.048% and 0.0012%, respectively, correspondingly the MAE are 0.42% and 0.075%, respectively. Figures 9(a) and 9(b) are shown for the measured and estimated battery terminal voltages under FUDS cycle, the red line in Figure 9(a) is the ARMA-based estimation value and the blue line denotes the IARMA-based estimation value. In Figure 9(b), the AAE of ARMA and IARMA are 0.058% and 0.0021%, respectively; correspondingly the MAE are 0.52% and 0.10%, respectively. As illustrated in Figures 8 and 9, the two model-based error stabilization of the terminal voltage has been achieved as continuous discharge, but it has small amplitude fluctuations. It means that the

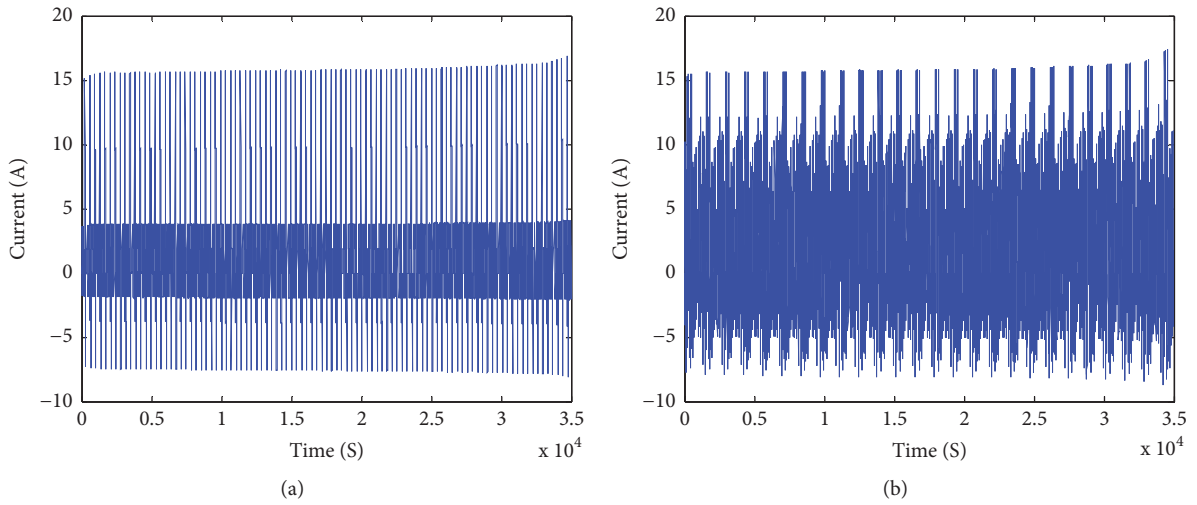

Figure 6: (a) Current under DST cycle; (b) current under FUDS cycle.

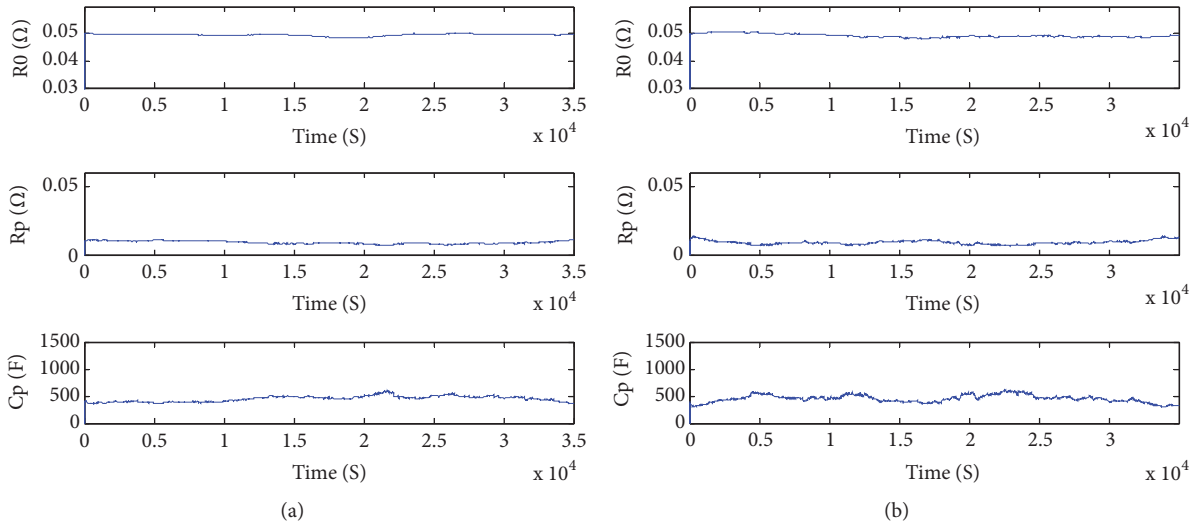

Figure 7: (a) Value of R_0, R_p, and C_p under DST cycle; (b) value of R_0, R_p, and C_p under FUDS cycle.

IARMA ECM and the ARMA ECM can both stably track the measurement value of the terminal voltage. The estimation error of the IARMA ECM is obviously decreased compared with the ARMA ECM. As summarized in Tables 1 and 2, the maximum terminal voltage error (MTVE) of the ARMA ECM is up to 109mV and 138mV under the DST and FUDS cycle, respectively; correspondingly the MTVE of the IARMA ECM is only 18 mV and 25mV under the DST and FUDS cycle, respectively. The average terminal voltage error of the IARMA ECM is only 0.35 mV and 1.3mV under the DST and FUDS cycle, respectively, which can be neglected regarding the sensors precision of the EVTS.

Besides, from (5) and (7), it can be inferred that the assumed RME indicates the effect of the OCV in the ARMA ECM is $(1 - a_1)V_{oc}(k)$. Similarly, the RME which defines the distribution of OCV with incremental analysis method in the IARMA ECM can be represented as $\Delta[V_{oc}(k) - a_1 V_{oc}(k - 1)]$. As the simulation results in Figure 10, the RME value of ARMA ECM is in a range from 0.6943 to 0.6941, and the maximum RME value of IARMA ECM is less than 0.03. By comparison with the Figures 10(a)–10(d), the RME

Table 1: Terminal voltage estimation under DST cycle.

Model	ARMA	IARMA
AAE (%)	0.048	0.0012
MAE (%)	0.42	0.075
MTVE (mV)	109	18

Table 2: Terminal voltage estimation under FUDS cycle.

Model	ARMA	IARMA
AAE (%)	0.058	0.0021
MAE (%)	0.52	0.10
MTVE (mV)	138	25

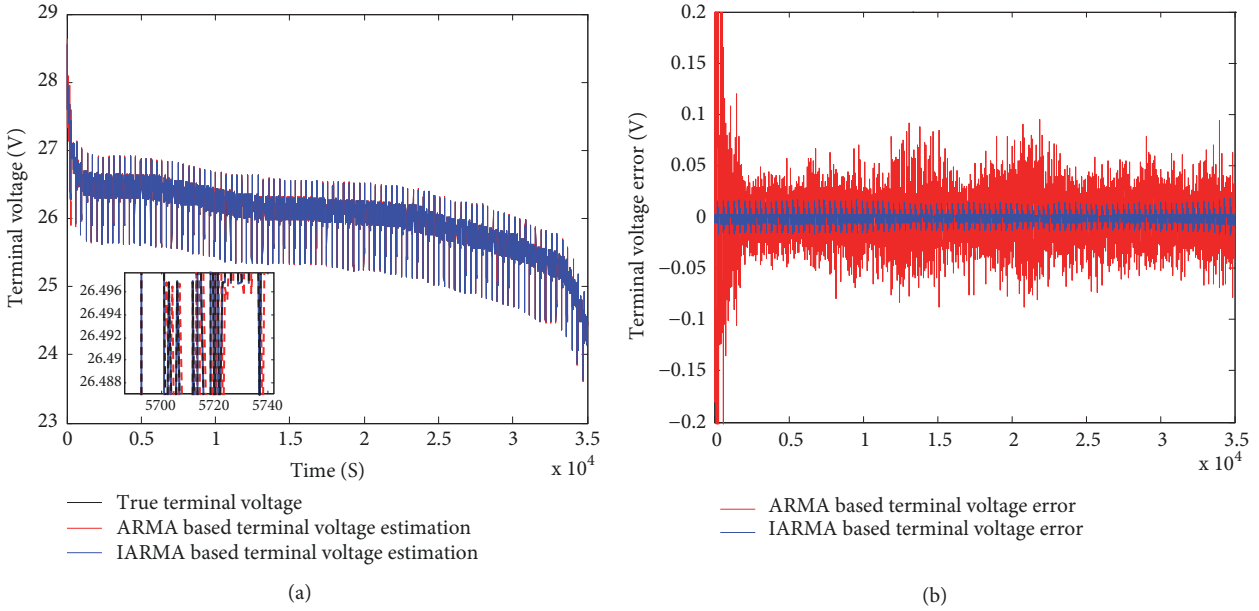

Figure 8: Terminal voltage under DST cycle with (a) estimation results; (b) estimation error.

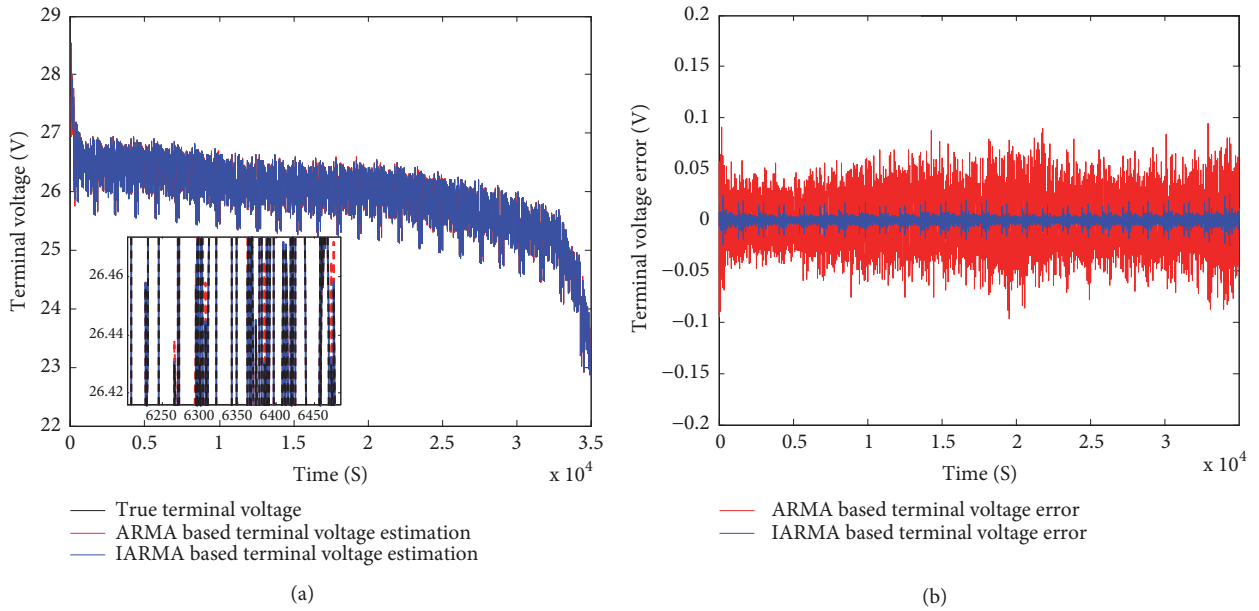

Figure 9: Terminal voltage under FUDS cycle with (a) estimation results; (b) estimation error.

in IARMA ECM is far smaller than that in ARMA ECM. Therefore, the proposed IARMA ECM can provide much better performance in parameters identification.

According to the above analysis, these comparing estimated results of the RME and terminal voltage error fully verify the capacity of the IARMA ECM to describe battery electric property. And the good performance further verifies the authenticity of the parameters identification strategy in practice.

5.2. SOC Estimation Results and Comparative Analysis. Two operation conditions including DST and FUDS are applied to evaluate the performance of SOC estimation method at 25°C. The reference SOC is calculated by coulomb counting (CC) method in EVTS and the reference SOC is used to approximate true value. As the testing battery in non-lab operation condition, it is difficult to obtain an accurate initial SOC value; thus, it is assumed that the initial SOC is set to 90% (with 10% initial error).

The two different models are compared in regard to the estimation result and error in Figure 11. The ARMA-based AHIF and IARMA-based AHIF are used to estimate the battery SOC and their tracking results are shown in

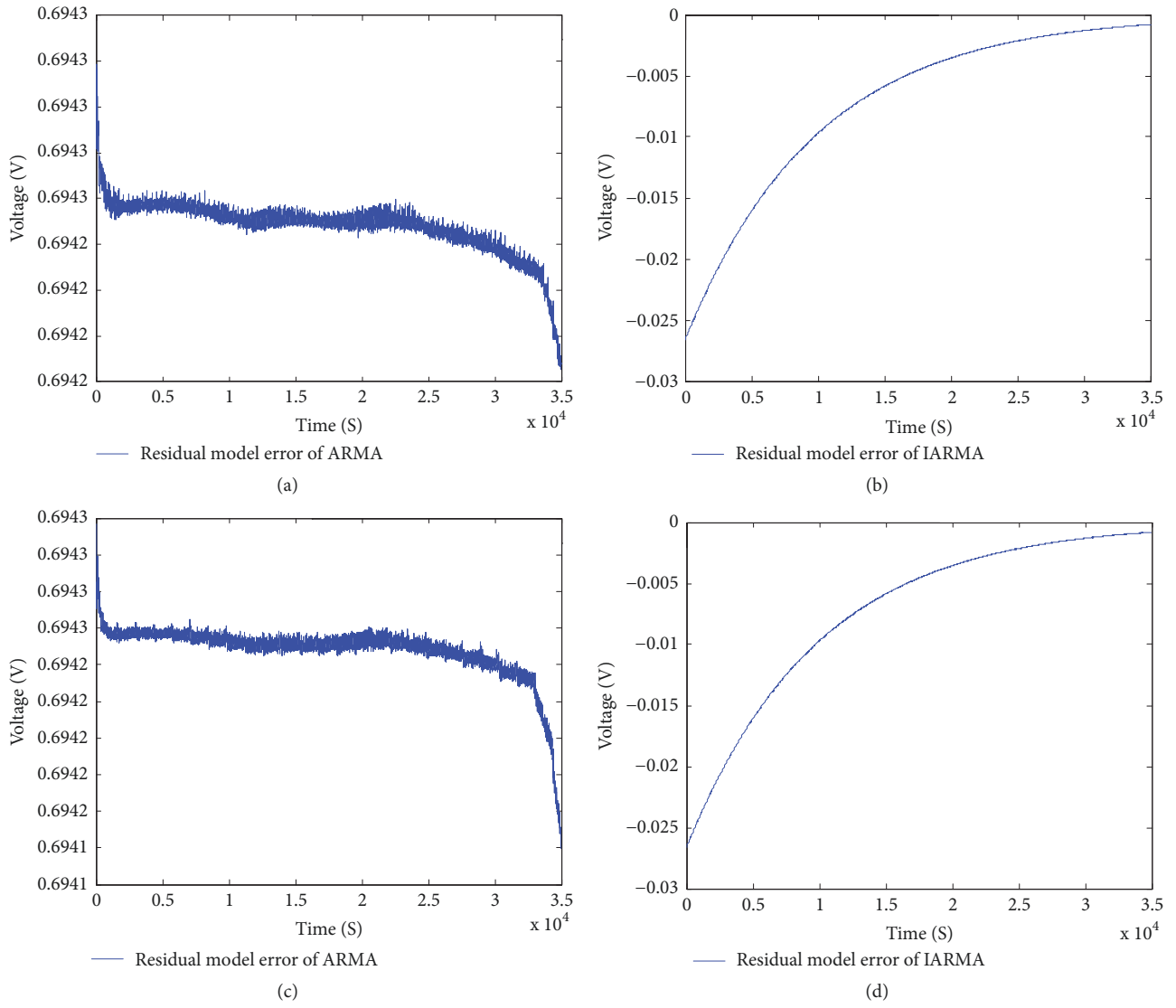

Figure 10: RME of (a) ARMA under DST cycle; (b) IARMA under DST cycle; (c) ARMA under FUDS cycle; (d) IARMA under FUDS cycle.

Figures 11(a)–11(d), where the black dashed-line presents the reference SOC with CC method and the red dotted-line represents the SOC estimation with ARMA-AHIF algorithm, while the blue solid-line indicates the SOC estimation with IARMA-AHIF algorithm. Among them, Figures 11(a) and 11(c) compare the observed SOC with the reference SOC and Figures 11(b) and 11(d) show the SOC estimation error in which the MAE is less than 1% except at the beginning of discharge. It shows that the two models based estimated SOC can both fast track the reference SOC at the inaccurate initial SOC. In particular, it is clear that the estimated SOC by proposed IARMA-based estimator has lower error in comparison with ARMA-based estimator since the former model can more accurately estimate the terminal voltage, and the difference between the measured and estimated terminal voltage causes a correction term to eliminate the SOC estimation error in a feedback control loop. In short, it is accordingly demonstrated that the IARMA-based AHIF algorithm can get a better SOC estimation than ARMA-based AHIF algorithm.

To further explore the promoting effects by error compensation strategy, the IARMA-based AHIF and corresponding error compensation (ΔOCV) are utilized to estimate the battery SOC and their tracking results are shown in Figures 12(a)–12(d), respectively, where the black dashed-line shows the reference SOC and the red dashed-line represents the SOC estimation with single AHIF algorithm, while the blue solid-line means the SOC estimation using AHIF-ΔOCV. Among them, Figures 12(a) and 12(c) compare the observed SOC with the reference SOC under DST and FUDS cycles, respectively; Figures 12(b) and 12(d) show the SOC estimation error between single AHIF and AHIF-ΔOCV under DST and FUDS cycles, respectively. The result shows that the above two algorithms can both rapidly track the reference SOC at the inaccurate initial SOC. It is worth noting that the AHIF-ΔOCV reduces the SOC estimation

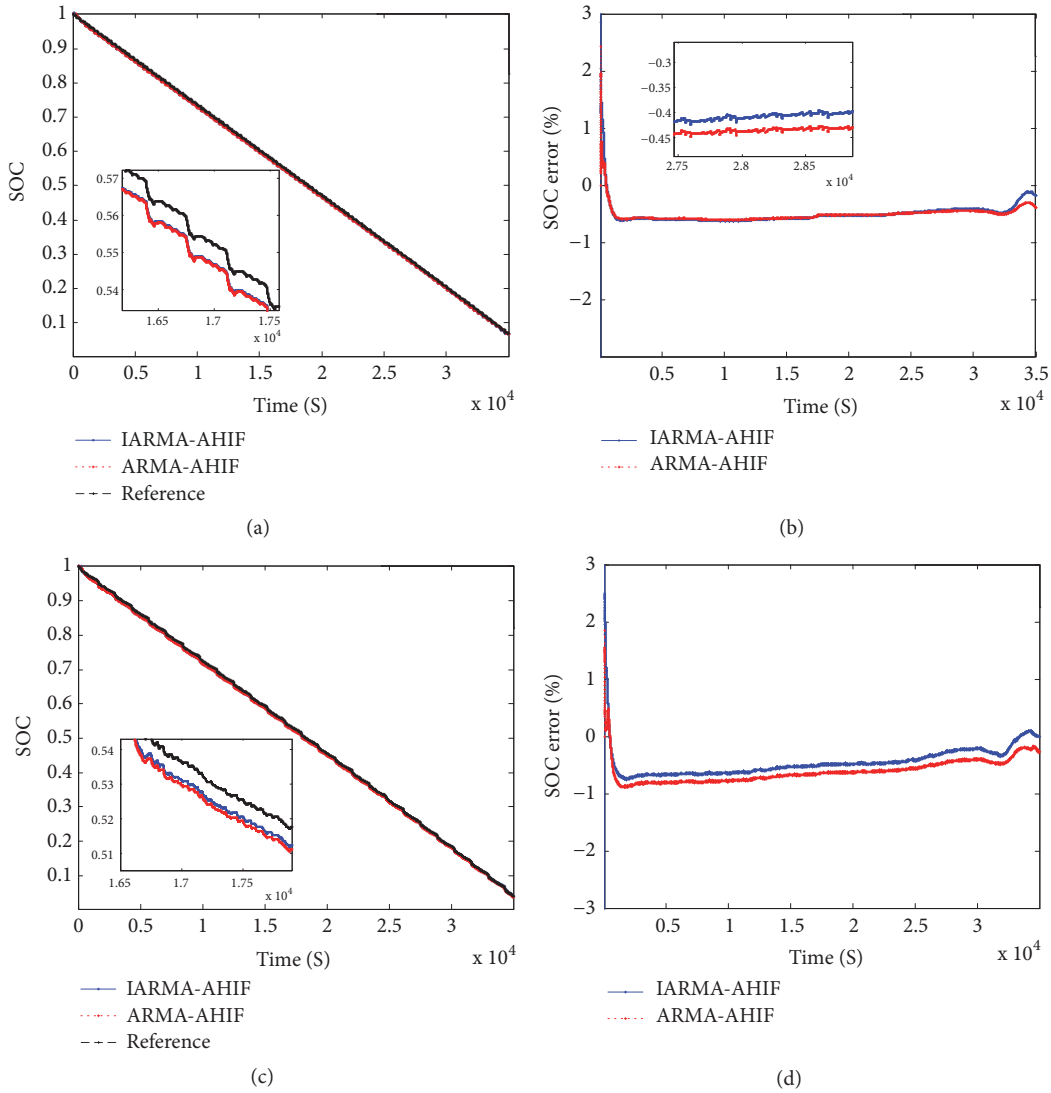

Figure 11: SOC estimation results: ARMA-AHIF versus IARMA-AHIF, (a) SOC under DST cycle; (b) SOC error under DST cycle; (c) SOC under FUDS cycle; (d) SOC error under FUDS cycle.

error significantly in comparison with single AHIF, in which the AAE of SOC estimation is decreased to 0.11% under DST cycle and to 0.18% under FUDS cycle, respectively. It can be concluded that the error compensation strategy is conducive to improving SOC estimation precision in AHIF algorithm.

Combining IARMA model and error compensation method in AHIF estimator, strengthening the robustness of SOC estimation is even more obvious. The AHIF-ΔOCV is compared with the AEKF-ΔOCV in terms of estimation precision and convergence. The comparison results, including tracking trajectory and estimation error under DST and FUDS cycles, are shown in Figure 13, where the black dashed-doted-line shows the reference SOC, the red dashed-line represents the SOC estimation using AEKF-ΔOCV, and the green doted-line denotes the SOC estimation using single AEKF, while the blue solid-line means the SOC estimation using AHIF-ΔOCV. As indicated in Figures 13(a) and 13(c), the SOC estimation results and reference SOC are subjected to DST and FUDS profile, respectively. The SOC estimation errors by those three algorithms are drawn in Figures 13(b) and 13(d). The estimated SOC by AHIF-ΔOCV tracks the reference SOC with a smoother path than by AEKF, which reflects the reliable correction capacity of the error compensation. The simulation results show that the three algorithms can always track the SOC reference trajectory after the convergence. Moreover, the comparison estimation results of the three algorithms mentioned above are summarized in Tables 3 and 4. From the new perspective on combining IARMA model and error compensation in AHIF and AEKF, an improvement of SOC estimation accuracy plays a certain significant role in the SOC estimation by Kalman filter family state observers.

6. Conclusion

As we all know that battery model uncertainty and OCV error have negative impacts on the battery SOC estimation. To overcome these shortcomings, the improved one-order ECM

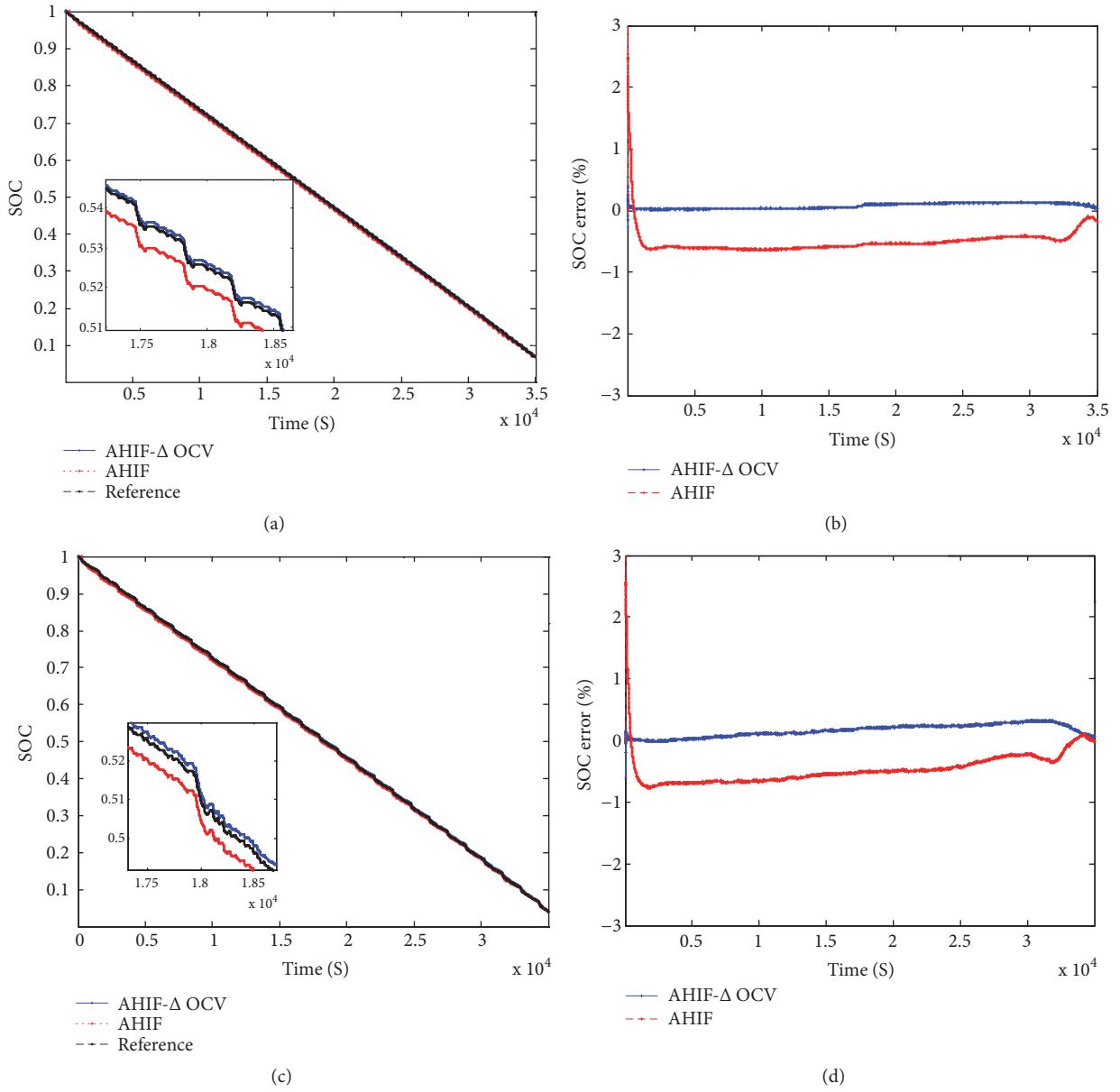

Figure 12: SOC estimation results: AHIF versus AHIF-ΔOCV, (a) SOC under DST cycle; (b) SOC error under DST cycle; (c) SOC under FUDS cycle; (d) SOC error under FUDS cycle.

Table 3: Comparison for the results under DST cycle.

Method	AEKF	AEKF-ΔOCV	AHIF-ΔOCV
AAE (%)	0.35	0.16	0.11
MAE (%)	1.84	0.68	0.54

Table 4: Comparison for the results under FUDS cycle.

Method	AEKF	AEKF-ΔOCV	AHIF-ΔOCV
AAE (%)	0.45	0.21	0.18
MAE (%)	2.44	0.73	0.59

based on IARMA analysis, independent OCV estimator, and adaptive H-Infinity Filter are proposed for SOC estimation. These methods include the following: (1) the RELS with variable forgetting factor for parameters identification is applied in IARMA model; (2) the independent OCV estimator with error compensation is adopted to accurately capture the OCV; (3) the high-precision SOC estimation is recursively obtained with improved AHIF including noise covariance and restricted factor adjustment. A high-precision experimental platform has been established to gather reliable data of charge/discharge current and terminal voltage. Two typical operation conditions (DST and FUDS) are adopted to evaluate the performance of parameters identification and state estimation. The simulation results indicate the favorable performances whose average SOC estimation error is only 0.11% (DST) and 0.18% (FUDS) by the proposed integrated method. As a model-based approach, the proposed

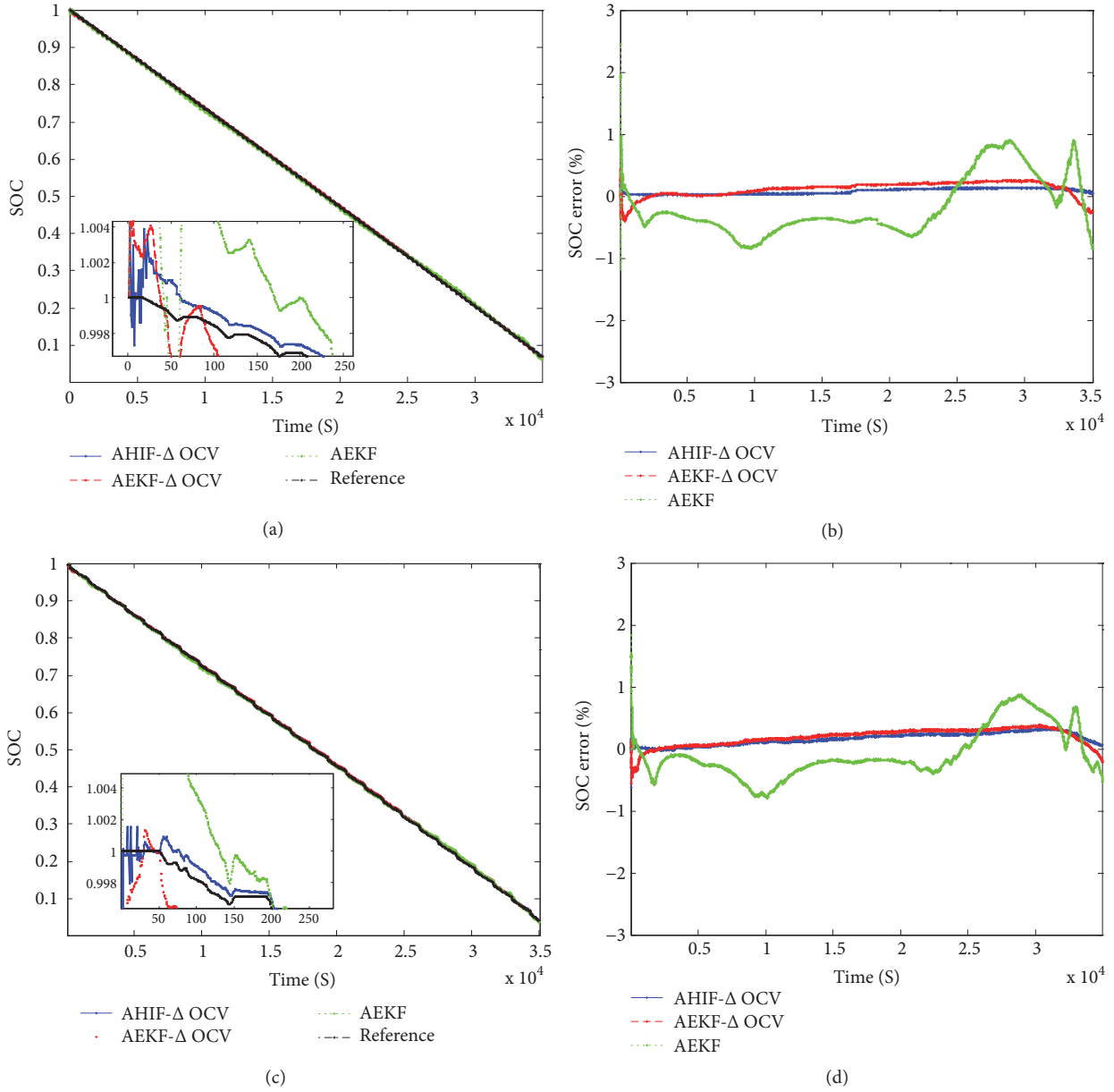

Figure 13: SOC estimation results: AEKF versus AEKF-ΔOCV versus AHIF-ΔOCV, (a) SOC under DST cycle; (b) SOC error under DST cycle; (c) SOC under FUDS cycle; (d) SOC error under FUDS cycle.

OCV-based SOC estimator is sensitive to the change of OCV-SOC curve. Therefore, the OCV-SOC will be considered as a normalized function including temperature and SOH in the future work. The OCV-SOC normalized function effectively updating is the key factor in the improvement of the precision and robustness of SOC estimator.

Data Availability

The data used to support the findings of this study are available from the corresponding author upon request.

Conflicts of Interest

The authors declare no conflicts of interest.

Authors' Contributions

Xuanju Dang and Zheng Liu proposed the original idea. Zheng Liu designed novel algorithm. Hanxu Sun, Xuanju Dang, and Zheng Liu performed and analyzed the experiments together. Zheng Liu wrote the original manuscript. Zheng Liu and Xuanju Dang revised the final manuscript.

Acknowledgments

This work was financially supported by the National Natural Science Foundation Project of China (61263013 and 61603107), Information Science Project of Guangxi Experiment Center (20130110), Guangxi Natural Science Foundation (2015GXNSFAA139297 and 2016GXNSFDA380001),

and Fundamental Ability Enhancement Project for Young and Middle-Aged University Teachers in Guangxi Province (2017KY0865).

References

[1] A. Farmann, W. Waag, A. Marongiu, and D. U. Sauer, "Critical review of on-board capacity estimation techniques for lithium-ion batteries in electric and hybrid electric vehicles," *Journal of Power Sources*, vol. 281, pp. 114–130, 2015.

[2] S. Han, B. Zhang, X. Sun, S. Han, and M. Höök, "China's Energy Transition in the Power and Transport Sectors from a Substitution Perspective," *Energies*, vol. 10, no. 5, p. 600, 2017.

[3] M. A. Hannan, M. M. Hoque, P. J. Ker, R. A. Begum, and A. Mohamed, "Charge equalization controller algorithm for series-connected lithium-ion battery storage systems: Modeling and applications," *Energies*, vol. 10, no. 9, 2017.

[4] J. Li, Q. Lai, L. Wang, C. Lyu, and H. Wang, "A method for SOC estimation based on simplified mechanistic model for LiFePO4 battery," *Energy*, vol. 114, pp. 1266–1276, 2016.

[5] K. Uddin, A. D. Moore, A. Barai, and J. Marco, "The effects of high frequency current ripple on electric vehicle battery performance," *Applied Energy*, vol. 178, pp. 142–154, 2016.

[6] B. Nastasi and G. Lo Basso, "Hydrogen to link heat and electricity in the transition towards future Smart Energy Systems," *Energy*, vol. 110, pp. 5–22, 2016.

[7] X. Q. Zhang, W. P. Zhang, H. Y. Li, and M. Zhang, "Review on state of charge estimation methods for li-ion batteries," *Transactions on Electrical and Electronic Materials*, vol. 18, pp. 136–140, 2017.

[8] K. S. Ng, C. S. Moo, Y. P. Chen, and Y. C. Hsieh, "Enhanced coulomb counting method for estimating state-of-charge and state-of-health of lithium-ion batteries," *Applied Energy*, vol. 86, no. 9, pp. 1506–1511, 2009.

[9] C. Weng, J. Sun, and H. Peng, "A unified open-circuit-voltage model of lithium-ion batteries for state-of-charge estimation and state-of-health monitoring," *Journal of Power Sources*, vol. 258, pp. 228–237, 2014.

[10] F. Zheng, Y. Xing, J. Jiang, B. Sun, J. Kim, and M. Pecht, "Influence of different open circuit voltage tests on state of charge online estimation for lithium-ion batteries," *Applied Energy*, vol. 183, pp. 513–525, 2016.

[11] H. Matsui, T. Nakamura, Y. Kobayashi, M. Tabuchi, and Y. Yamada, "Open-circuit voltage study on LiFePO4 olivine cathode," *Journal of Power Sources*, vol. 195, no. 19, pp. 6879–6883, 2010.

[12] L. Kang, X. Zhao, and J. Ma, "A new neural network model for the state-of-charge estimation in the battery degradation process," *Applied Energy*, vol. 121, pp. 20–27, 2014.

[13] J. Kim, S. Lee, and B. H. Cho, "Discrimination of Li-ion batteries based on Hamming network using discharging-charging voltage pattern recognition for improved state-of-charge estimation," *Journal of Power Sources*, vol. 196, no. 4, pp. 2227–2240, 2011.

[14] T. Wu, M. Wang, Q. Xiao, and X. Wang, "The SOC Estimation of Power Li-Ion Battery Based on ANFIS Model," *Smart Grid and Renewable Energy*, vol. 03, no. 01, pp. 51–55, 2012.

[15] S. Sepasi, L. R. Roose, and M. M. Matsuura, "Extended Kalman filter with a fuzzy method for accurate battery pack state of charge estimation," *Energies*, vol. 8, no. 6, pp. 5217–5233, 2015.

[16] H. Sheng and J. Xiao, "Electric vehicle state of charge estimation: Nonlinear correlation and fuzzy support vector machine," *Journal of Power Sources*, vol. 281, pp. 131–137, 2015.

[17] V. Klass, M. Behm, and G. Lindbergh, "Capturing lithium-ion battery dynamics with support vector machine-based battery model," *Journal of Power Sources*, vol. 298, pp. 92–101, 2015.

[18] X. Dang, L. Yan, H. Jiang, X. Wu, and H. Sun, "Open-circuit voltage-based state of charge estimation of lithium-ion power battery by combining controlled auto-regressive and moving average modeling with feedforward-feedback compensation method," *International Journal of Electrical Power & Energy Systems*, vol. 90, pp. 27–36, 2017.

[19] X. Dang, L. Yan, K. Xu, X. Wu, H. Jiang, and H. Sun, "Open-Circuit Voltage-Based State of Charge Estimation of Lithium-ion Battery Using Dual Neural Network Fusion Battery Model," *Electrochimica Acta*, vol. 188, pp. 356–366, 2016.

[20] X. Lai, Y. Zheng, and T. Sun, "A comparative study of different equivalent circuit models for estimating state-of-charge of lithium-ion batteries," *Electrochimica Acta*, vol. 259, pp. 566–577, 2018.

[21] T. Feng, L. Yang, X. Zhao, H. Zhang, and J. Qiang, "Online identification of lithium-ion battery parameters based on an improved equivalent-circuit model and its implementation on battery state-of-power prediction," *Journal of Power Sources*, vol. 281, pp. 192–203, 2015.

[22] Y. Li, L. Wang, C. Liao, L. Wang, and D. Xu, "Recursive modeling and online identification of lithium-ion batteries for electric vehicle applications," *Science China Technological Sciences*, vol. 57, no. 2, pp. 403–413, 2014.

[23] Y. Wang, C. Zhang, and Z. Chen, "An adaptive remaining energy prediction approach for lithium-ion batteries in electric vehicles," *Journal of Power Sources*, vol. 305, pp. 80–88, 2016.

[24] C. Song, Y. Shao, S. Song et al., "Insulation resistance monitoring algorithm for battery pack in electric vehicle based on extended kalman filtering," *Energies*, vol. 10, no. 6, p. 714, 2017.

[25] Z. W. He, M. Y. Gao, C. S. Wang, L. Y. Wang, and Y. Liu, "Adaptive state of charge estimation for Li-ion batteries based on an unscented kalman filter with an enhanced battery model," *Energies*, vol. 6, no. 8, pp. 4134–4151, 2013.

[26] P. Tagade, K. S. Hariharan, P. Gambhire et al., "Recursive Bayesian filtering framework for lithium-ion cell state estimation," *Journal of Power Sources*, vol. 306, pp. 274–288, 2016.

[27] Y. Li, C. Wang, and J. Gong, "A multi-model probability SOC fusion estimation approach using an improved adaptive unscented Kalman filter technique," *Energy*, vol. 141, pp. 1402–1415, 2017.

[28] F. Sun, R. Xiong, and H. He, "Estimation of state-of-charge and state-of-power capability of lithium-ion battery considering varying health conditions," *Journal of Power Sources*, vol. 259, pp. 166–176, 2014.

[29] S. P. Bhattacharyya, "Robust control under parametric uncertainty: An overview and recent results," *Annual Reviews in Control*, vol. 44, pp. 45–77, 2017.

[30] O. Gazi, *Understanding digital signal processing*, vol. 13 of *Springer Topics in Signal Processing*, Springer, Singapore, 2018.

[31] H. K. Sahoo and P. K. Dash, "Robust estimation of power quality disturbances using unscented H1 filter," *Electrical Power and Energy Systems*, vol. 73, pp. 438–447, 2015.

[32] Y. Zhang, R. Xiong, H. He, and W. Shen, "Lithium-Ion Battery Pack State of Charge and State of Energy Estimation Algorithms Using a Hardware-in-The-Loop Validation," *IEEE Transactions on Power Electronics*, vol. 32, no. 6, pp. 4421–4431, 2017.

[33] C. Chen, R. Xiong, and W. Shen, "A Lithium-Ion Battery-in-the-Loop Approach to Test and Validate Multiscale Dual H Infinity Filters for State-of-Charge and Capacity Estimation," *IEEE Transactions on Power Electronics*, vol. 33, no. 1, pp. 332–342, 2018.

[34] M. Charkhgard and M. H. Zarif, "Design of adaptive H_∞ filter for implementing on state-of-charge estimation based on battery state-of-charge-varying modeling," *IET Power Electronics*, vol. 8, pp. 1825–1833, 2015.

[35] C. Lin, Q. Yu, R. Xiong, and L. Y. Wang, "A study on the impact of open circuit voltage tests on state of charge estimation for lithium-ion batteries," *Applied Energy*, vol. 205, pp. 892–902, 2017.

[36] H. Wu, S. Yuan, X. Zhang, C. Yin, and X. Ma, "Model parameter estimation approach based on incremental analysis for lithium-ion batteries without using open circuit voltage," *Journal of Power Sources*, vol. 287, pp. 108–118, 2015.

[37] Z. Wei, K. J. Tseng, N. Wai, T. M. Lim, and M. Skyllas-Kazacos, "Adaptive estimation of state of charge and capacity with online identified battery model for vanadium redox flow battery," *Journal of Power Sources*, vol. 332, pp. 389–398, 2016.

[38] Y. Wang, C. Zhang, and Z. Chen, "On-line battery state-of-charge estimation based on an integrated estimator," *Applied Energy*, vol. 185, pp. 2026–2032, 2017.

[39] C. Zhang, W. Allafi, Q. Dinh, P. Ascencio, and J. Marco, "Online estimation of battery equivalent circuit model parameters and state of charge using decoupled least squares technique," *Energy*, vol. 142, pp. 678–688, 2018.

[40] H. Dai, T. Xu, L. Zhu, X. Wei, and Z. Sun, "Adaptive model parameter identification for large capacity Li-ion batteries on separated time scales," *Applied Energy*, vol. 184, pp. 119–131, 2016.

[41] X. Chen, W. Shen, M. Dai, Z. Cao, J. Jin, and A. Kapoor, "Robust adaptive sliding-mode observer using RBF neural network for lithium-ion battery state of charge estimation in electric vehicles," *IEEE Transactions on Vehicular Technology*, vol. 65, no. 4, pp. 1936–1947, 2016.

[42] Y. Naderahmadian, M. A. Tinati, and S. Beheshti, "Generalized adaptive weighted recursive least squares dictionary learning," *Signal Processing*, vol. 118, pp. 89–96, 2016.

[43] M. Badoni, A. Singh, and B. Singh, "Variable forgetting factor recursive least square control algorithm for DSTATCOM," *IEEE Transactions on Power Delivery*, vol. 30, no. 5, pp. 2353–2361, 2015.

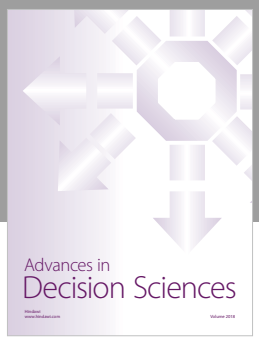

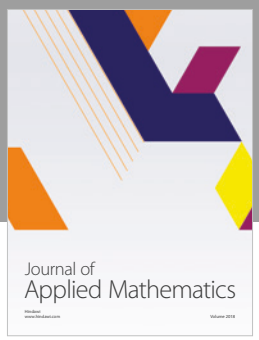

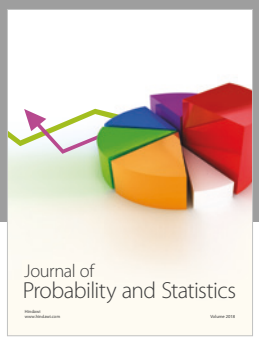

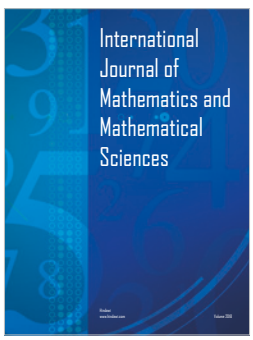

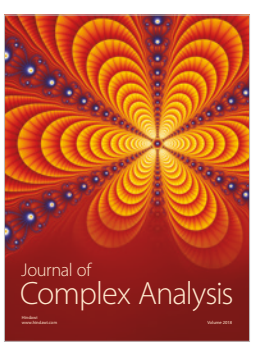

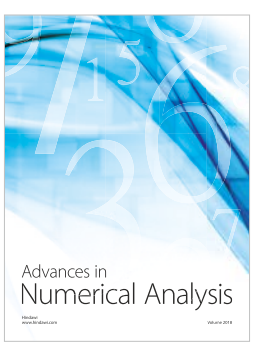

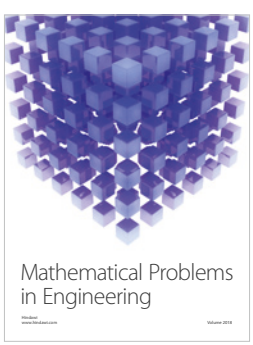

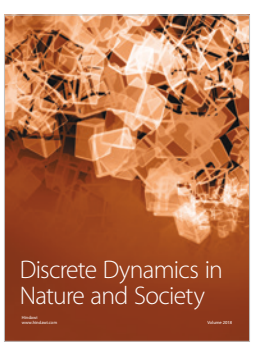

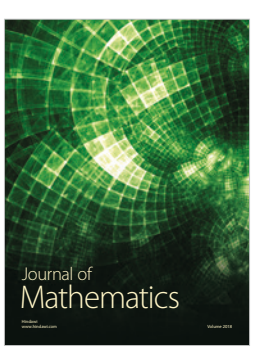

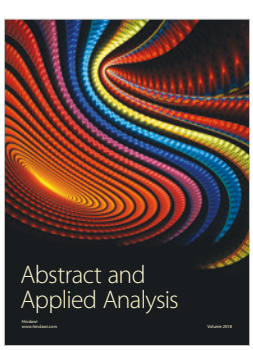

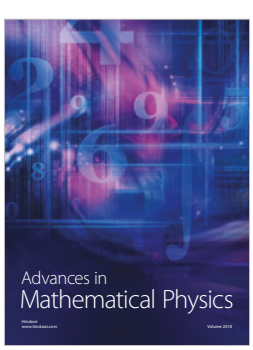

Hindawi

Submit your manuscripts at
www.hindawi.com